PRAMANA
— journal of
physics

Vol. 65, No. 5
November 2005
pp. 937–947

Nanoparticles of complex metal oxides synthesized using the reverse-micellar and polymeric precursor routes

ASHOK K GANGULI*, TOKEER AHMAD, PADAM R ARYA and PIKA JHA
Department of Chemistry, Indian Institute of Technology Delhi, New Delhi 110 016, India
*Corresponding author. E-mail: ashok@chemistry.iitd.ernet.in

Abstract. Current interest in the properties of materials having grains in the nanometer regime has led to the investigation of the size-dependent properties of various dielectric and magnetic materials. We discuss two chemical methods, namely the reverse-micellar route and the polymeric citrate precursor route used to obtain homogeneous and monophasic nanoparticles of several dielectric oxides like $BaTiO_3$, Ba_2TiO_4, $SrTiO_3$, $PbTiO_3$, $PbZrO_3$ etc. In addition we also discuss the synthesis of some transition metal (Mn and Cu) oxalate nanorods using the reverse-micellar route. These nanorods on decomposition provide a facile route to the synthesis of transition metal oxide nanoparticles. We discuss the size dependence of the dielectric and magnetic properties in some of the above oxides.

Keywords. Chemical synthesis; nanoparticle; transmission electron microscopy; dielectric properties.

PACS Nos 81.07.Bc; 77.84.Dy; 82.70.Uv; 75.50.-y

1. Introduction

$BaTiO_3$ and lead zirconium titanate, $PbZr_xTi_{1-x}O_3$ (PZT), are well-known ferroelectric materials for piezoelectric, electro-optic, pyroelectric applications and are also useful as ferroelectrics in non-volatile random access memories [1–6]. Barium strontium titanates $Ba_{1-x}Sr_xTiO_3$ (BST) are important due to their application in tunable filters, oscillators and phase elements in antennas [7].

For increased miniaturization and volumetric efficiency of these multilayer capacitors, the thickness of the ceramic capacitor films has to be decreased and hence nanocrystalline dielectric oxides are important. It would be easy to densely pack these nanoparticles to yield sintered ceramics with little void space and less cracks. It is of interest to investigate the effect of grain-size reduction on the dielectric properties. There have been very limited efforts in the area of dielectric nanomaterials when compared to other nanostructured materials (magnetic, optical, catalytic). A few reports discuss the dielectric properties observed in nanosized particles of related oxides like $BaTiO_3$ [8,9] and $SrTiO_3$ [9,10].

Magnetic properties of nanosized oxides are important due to the technological requirements of these materials in recording media and disks. New devices like spin-valves, spin-transistors, magnetocaloric refrigeration systems, ferrofluid technology etc. rely on magnetic properties of nanocrystalline solids.

There have been several studies on the synthesis of oxides by low-temperature routes to obtain relatively homogeneous and small-sized grains. These methods include chemical co-precipitation [11], hydrothermal reaction [12] and the sol–gel method [13,14]. Here we discuss two low-temperature synthetic routes (polymeric precursor and reverse-micellar) other than the methods mentioned above. Our emphasis here is to obtain uniform and pure nanomaterials by efficient synthetic strategies. In this article we concentrate on some of our studies on the synthesis and properties of dielectric (barium titanate-related) and magnetic nanomaterials (copper and manganese oxides). The common theme is to understand the size-effect on ordered electric dipole moments in the case of dielectric materials or ordered magnetic dipoles in the case of magnetic materials.

2. Synthetic methodologies

We have used two chemical routes for the synthesis of nanoparticles: (1) the polymeric precursor method and (2) the reverse-micellar route. The polymeric citrate method is based on the Pechini-type reaction route [15,16]. It involves reacting a mixed solution of citric acid, ethylene glycol and the desired cations to form a polyester type of gel. The metal ions can be immobilized in a rigid polyester network, which is charred off by heating the gel. This can greatly reduce the diffusion path lengths of a particular reactant during the processing. Thus a distinct advantage over most other methods is that very pure mixed metal oxides can be prepared. Also compared to the ceramic route, this method can give rise to homogeneous and fine-grained powders at relatively lower reaction temperatures. We have used the polymeric citrate precursor to synthesize nanoparticles of well-known ABO_3-type oxides, e.g., $Ba_{1-x}Sr_xTiO_3$ [17] and $Ba_{1-x}Pb_xTiO_3$ [18] (see references for experimental details).

The reverse-micellar route using microemulsions to produce nanomaterials has been known for sometime [19], but the mechanism to control the size distribution and final size of the product is not yet completely known. Microemulsions are optically transparent and thermodynamically stable dispersions of two immiscible liquids (like water and oil) which are stabilized by a surfactant. The size of the reverse micelle (droplets of water in oil) can be controlled by varying the ratio of $R =$ [water or oil]/[surfactant] in the nanometer range. It is possible to control not only the size but also the morphology of the product nanoparticles by proper choice of the composition of the microemulsion system. The mixing of microemulsions containing different ions in the aqueous core results in the coalescence of droplets and interchange of reactants resulting in the reaction inside a small volume (nanoreactors) (figure 1). The synthetic procedure to obtain nanosized $BaTiO_3$ by the reverse micellar route is given elsewhere [20].

The synthesis of the transition metal oxide nanoparticles was carried out in two steps. First, we synthesized the nanorods of metal oxalate from two microemulsions. In the second step, the metal oxalate particles were subjected to a careful thermal

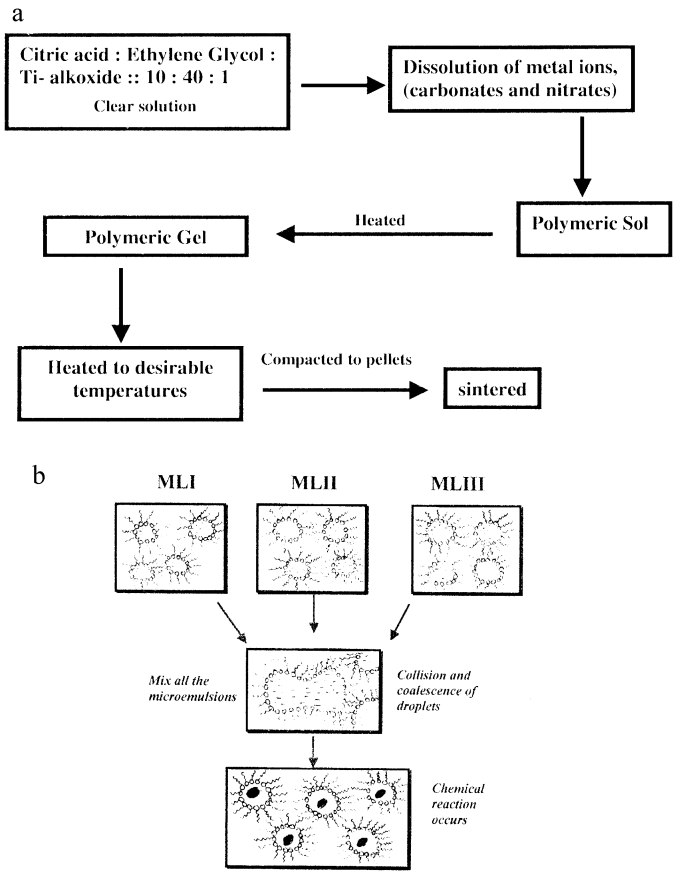

Figure 1. Schematic representation of the experimental procedure followed for the synthesis of $BaTiO_3$ by (**a**) polymeric precursor method and (**b**) reverse-micellar route.

decomposition to yield nanoparticulate oxide [21]. All the nanocrystalline powders were characterized by a variety of techniques (XRD, TEM, dielectric and magnetic measurement) [20–22].

3. Results and discussion

3.1 *Dielectric oxides obtained by the polymeric precursor route*

Monophasic oxides of the type, $Ba_{1-x}Sr_xTiO_3$, were obtained after heating the precursors (prepared by the polymeric citrate precursor route) at 500°C. The powder X-ray diffraction patterns could be indexed on the basis of a cubic cell as known for cubic $BaTiO_3$. It is seen that there is a decrease in the a lattice parameter with increase in strontium substitution, which is expected, since Sr^{2+} has a smaller ionic radius than Ba^{2+}. The gel (formed after 135°C heating) and the precursor (formed

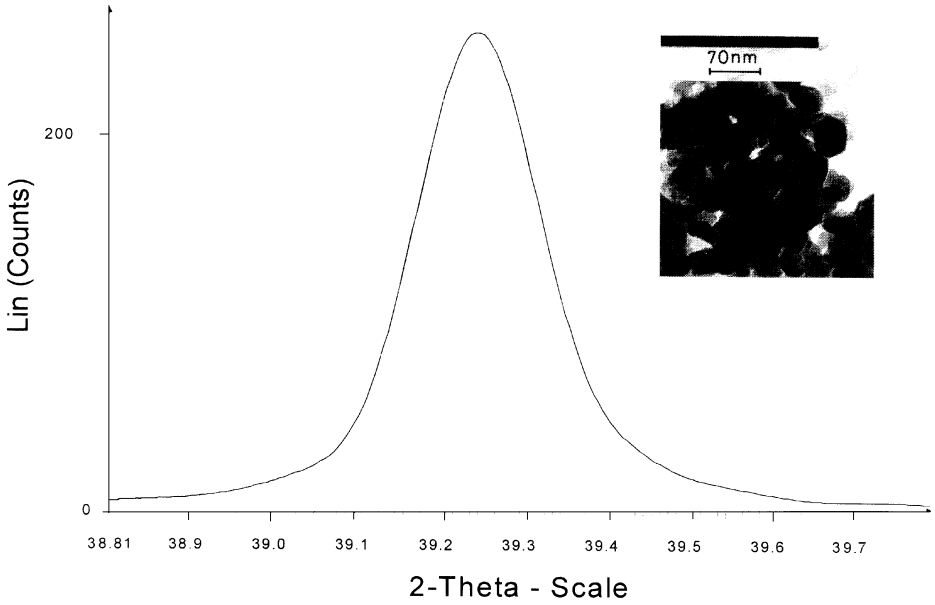

Figure 2. Slow scan (PXRD) of 1 1 1 reflection for line broadening studies (after heating at 500°C) and inset shows the transmission electron micrograph of $PbTiO_3$.

after 300°C heating) show amorphous nature as observed from the powder X-ray diffraction studies. It is found that after sintering at 1100°C, $BaTiO_3$ is weakly tetragonal ($c/a = 1.0027$) while all the other compositions are cubic. A careful analysis of the powder X-ray diffraction data for $SrTiO_3$ shows that at 1100°C it disproportionates to its higher homologue $Sr_4Ti_3O_{10}$ [17].

Oxides of the type $Ba_{1-x}Pb_xTiO_3$ were obtained from the gel at 500°C. The powder X-ray diffraction patterns could be indexed on the basis of a tetragonal cell for all the compositions. For $PbTiO_3$ the tetragonal lattice parameters were $a = 3.899(1)$ Å, $c = 4.136(2)$ Å. The a parameter decreases whereas the c parameter increases with increase in lead content [18].

The particle size of all the above oxides have been found to be in the nanoregime as is evident from line broadening studies of X-ray as well as transmission electron microscopy (TEM). We observe a distribution of grain sizes with most of the grains in the range of 20 to 30 nm for $SrTiO_3$. The particle size obtained for $SrTiO_3$ sintered at 1100°C is found to be 88 nm [17]. This shows that with sintering there is only a marginal increase in grain size even at a high temperature. A grain size of 50 nm for $PbTiO_3$ (figure 2) is observed [18] using the Scherrer's formula. The particle size obtained from TEM (inset of figure 2) is in the range of 40–60 nm for barium lead oxides and corroborate well with the X-ray line broadening studies.

The dielectric properties of all these oxides have been studied in detail with respect to variation in frequency and temperature. The dielectric constant varies from 510 for $BaTiO_3$ to 190 for $SrTiO_3$. These samples were sintered at 1100°C and the density of these disks was 95–96%. The dielectric loss (D) is nearly constant

till 200 kHz (0.002). The dielectric constant of $BaTiO_3$ (sintered at 1100°C) shows reasonable stability till 150°C. All the lead-doped phases (sintered at 900°C) show dielectric constant in the region of 30 to 80 at 100 kHz. The dielectric loss for different compositions is found to vary between 0.005 and 0.10.

3.2 *Oxides obtained by the reverse-micellar route*

We discuss the synthesis of $BaTiO_3$, Ba_2TiO_4, CuO, MnO, Mn_2O_3 and Mn_3O_4 by the reverse micellar route. Monophasic $BaTiO_3$ could be obtained [20] after heating the precursor at 800°C and the X-ray diffraction pattern could be indexed satisfactorily on the basis of a tetragonal cell with refined lattice parameters $a = 3.998(1)$ Å and $c = 4.019(1)$ Å. X-ray line broadening studies show an average grain size of 30 nm (figure 3). This is in accordance with the transmission electron microscopic studies (TEM) which show particles with 25–30 nm grain size (figure 3, inset). The X-ray diffraction pattern indicates the presence of weak tetragonal distortion of $BaTiO_3$. This distortion was confirmed by carrying out Raman spectroscopic studies [20]. The grain size was found to be 40 nm for $BaTiO_3$ (sintered disk at 900°C). TEM micrographs showed agglomerated particles of grain size of the order of 80–100 nm after sintering at 1100°C. Thus there is a marginal increase in grain size with sintering temperature (from ∼30 nm to ∼100 nm). Note that the grain size of $BaTiO_3$ obtained by the ceramic route at 1100°C normally varies between 0.5 and 1 μm.

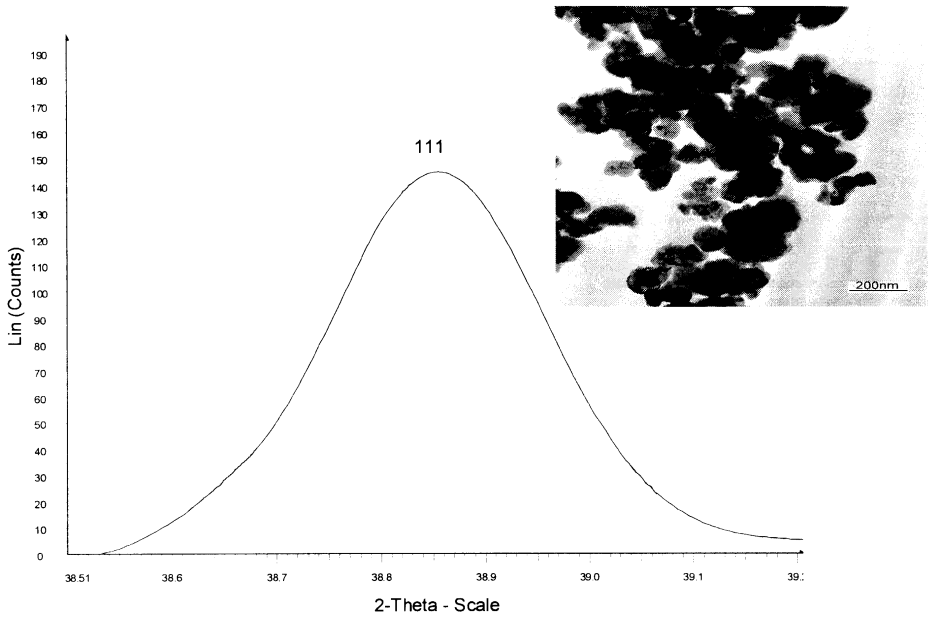

Figure 3. Slow scan XRD studies of 1 1 1 reflection for line broadening studies for $BaTiO_3$ heated at 800°C. Inset shows the transmission electron micrograph.

The dielectric constant and dielectric loss were measured on sintered disks (900°C) of the nanostructured barium titanate as a function of frequency and temperature. The dielectric constant was found to be 220 and dielectric loss was 0.023 for $BaTiO_3$ at 100 kHz. The dielectric constant was found to be stable ($d\varepsilon/dF = 8.76 \times 10^{-7}$ Hz^{-1}) with frequency while dielectric loss showed a slight increase at higher frequencies. Measurement of dielectric properties of nanosized $BaTiO_3$ was also carried out after sintering at 1100°C. The dielectric constant is found to increase with sintering temperature (being 560) after sintering at 1100°C. The dielectric loss shows a decrease with sintering temperature. This decrease in loss is normally associated with increase in grain size. The dielectric loss was nearly constant with frequency (0.02) after the 1100°C sintering. The dielectric constant is among the highest reported for nanostructured $BaTiO_3$ obtained by different routes [17]. In the temperature variation of the dielectric data (figure 4), we find a small hump in the dielectric constant/loss near 140–150°C. This feature may be associated with the ferroelectricity of $BaTiO_3$. Bulk $BaTiO_3$ (micron size grains) is a ferroelectric material with a transition temperature of 122°C. Ferroelectricity is highly dependent on grain size and a critical size of ∼44 nm was suggested earlier by theoretical calculations [23]. However, more recently it has been shown that ferroelectricity may be observed in defect-free ultra-thin films [24] much below (<10 nm) the limits normally suggested by a mean-field Ginzburg–Landau approach.

Nanoparticles of barium orthotitanate (Ba_2TiO_4) have also been obtained [22] using microemulsions (avoiding Ba-alkoxide) by a similar method as used for $BaTiO_3$. Powder X-ray diffraction studies of the powder after calcining at 800°C result in a mixture of orthorhombic (70%) and monoclinic (30%) phases. The high-temperature orthorhombic form present at 800°C is probably due to the small size of particles obtained by the reverse-micellar route. Pure orthorhombic Ba_2TiO_4 was obtained on further sintering at 1000°C with lattice parameters,

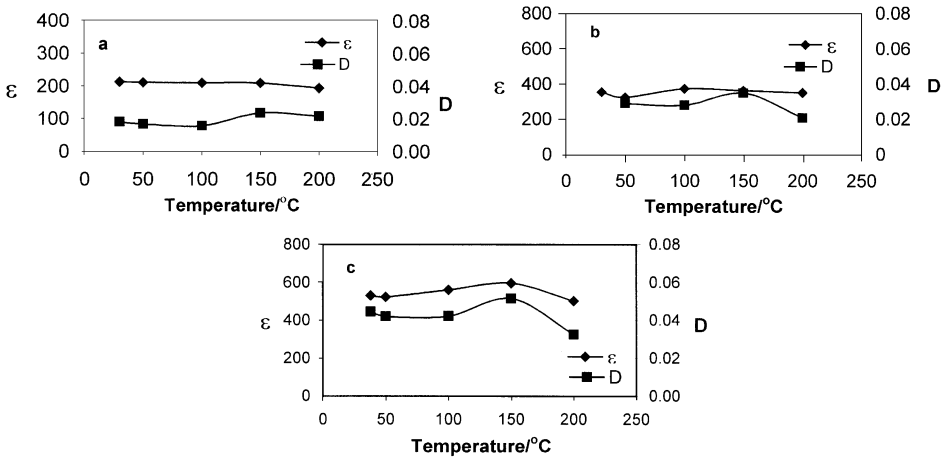

Figure 4. Variation of dielectric constant (ε) and dielectric loss (D) with temperature at 100 kHz for samples sintered at (**a**) 900°C, (**b**) 1000°C and (**c**) 1100°C.

$a = 6.101(2)$ Å, $b = 22.94(1)$ Å and $c = 10.533(2)$ Å (space group, $P2_1nb$). The grain size obtained from careful line broadening studies comes out to be 46 nm. TEM studies show agglomerated grains (40–50 nm) at 800°C (figure 5a). Thus our TEM studies conform well with that of the line broadening studies. Sintering at 1000°C shows increase in grain size up to 150 nm (figure 5b). Our studies corroborate well with the presence of a martensitic transition in Ba_2TiO_4. The dielectric constant is found to be 40 for Ba_2TiO_4 (at 100 kHz) for samples sintered at 1000°C. The dielectric loss obtained was low (0.06) at 100 kHz.

Among the various magnetic oxides synthesized by us using the reverse-micellar route, we discuss the synthesis and properties of copper and manganese oxides. The precursor obtained by centrifugation of the microemulsion mixture leads to the formation of copper oxalate monohydrate [25]. On further heating this precursor at 450°C, pure CuO is obtained. Scanning electron micrograph of the sample of copper oxalate monohydrate shows nanorods of 150 nm diameter and 700 nm length

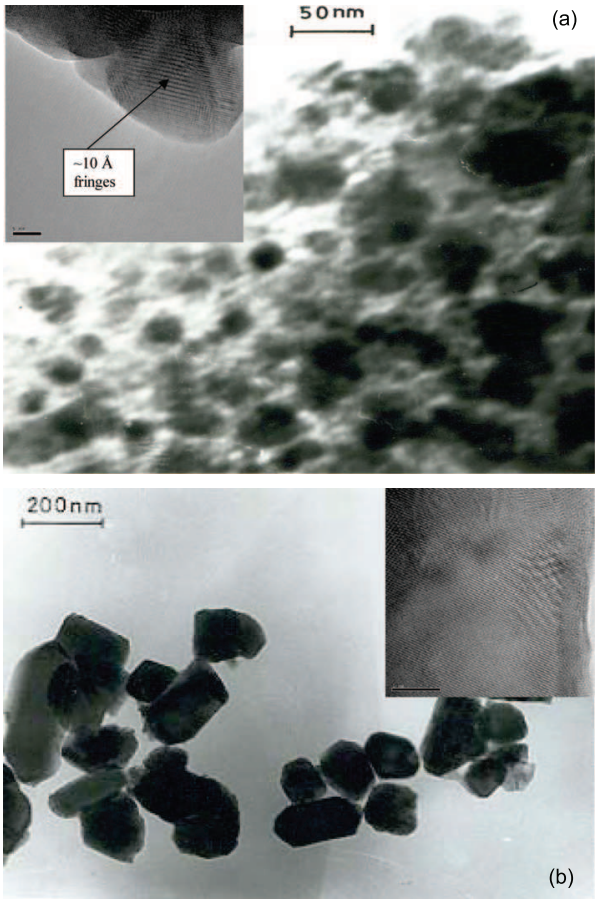

Figure 5. Transmission electron micrograph of Ba_2TiO_4 at (**a**) 800°C and (**b**) 900°C. Inset shows their respective HRTEM images.

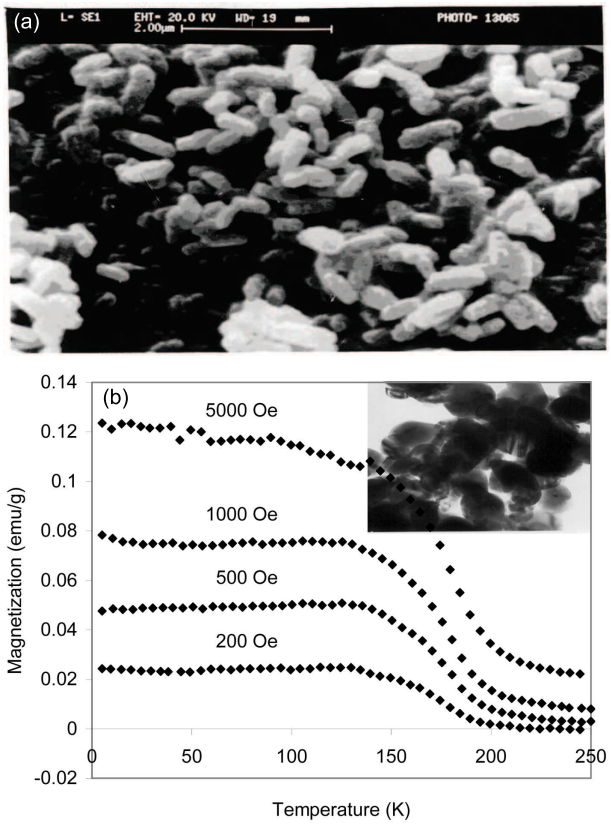

Figure 6. (**a**) SEM micrograph of copper oxalate monohydrate nanorods and (**b**) temperature dependence of the magnetization of CuO nanoparticles. Inset shows the TEM picture of CuO nanoparticles.

(figure 6a). In contrast to nanorods, nearly spherical particles of the order of 80 nm were obtained for copper oxide (figure 6b, inset). By varying the non-aqueous medium in the microemulsion we could obtain particles of different sizes. The temperature dependence of the magnetization at several fields for the copper oxide nanoparticles is shown in figure 6b. One notices a jump in the magnetization of the CuO nanoparticles near 220 K [25], approximately the value of the Neél temperature of bulk CuO. The non-zero magnetization in the antiferromagnetic state has been attributed to spin canting [26]. It has been pointed out that the magnetization is non-linear in field even above T_N, remaining nearly independent of temperature [27]. This has been attributed to short-range antiferromagnetic correlation [28]. The independence of the magnetization at high temperatures on particles gives an indication of the robustness of the correlation (recall that the susceptibility is nearly constant up to 1000 K) [27]. These results also show the difficulty in attaining long-range ordering despite the intensity of the short-range correlation. It is interesting to note that our sample, except at the very lowest temperature, shows no sign of 'paramagnetic impurities. A large Curie-like susceptibility has been

observed in some sintered samples and has been attributed to oxygen vacancies, creating Cu^{1+} ions [29,30], and the presence of CuO particles which are too small to allow long-range magnetic order [27]. The present results seem to confirm the former supposition, because our smallest nanoparticles show only reduced ordering temperature and not Curie-like behaviour.

Anhydrous manganese oxalate nanorods have also been synthesized by the microemulsion route as discussed for copper oxalate nanorods. The powder X-ray diffraction pattern of the manganese oxalate nanorods is indexed on the basis of an orthorhombic cell with the refined unit cell parameters ($a = 7.158(7)$, $b = 5.873(4)$, $c = 9.020(9)$ Å). Transmission electron microscopic studies showed the formation of nanorods of manganese oxalate with average dimensions of 100 nm diameter and 2.5 μm length (figure 7a). On the basis of the TGA/DTA studies, we calcined the precursor (obtained by the reverse-micellar route) at 450–500°C for 6–12 h. Annealing of the manganese oxalate nanorods in vacuum, air and nitrogen led to MnO, α-Mn_2O_3 and Mn_3O_4 respectively [21].

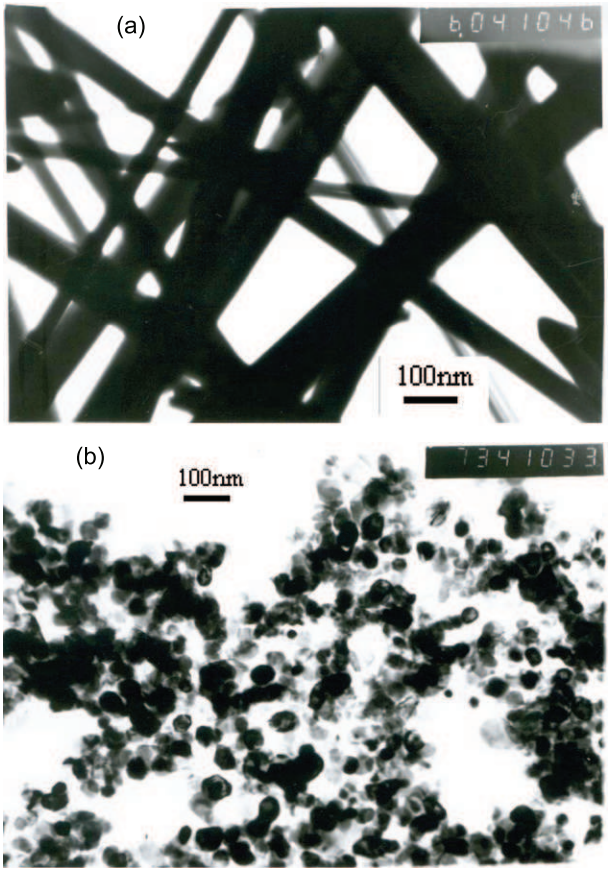

Figure 7. TEM micrographs of (**a**) manganese oxalate nanorods and (**b**) MnO nanoparticles.

All the oxides were found to be monophasic and had grains in the range of 30–50 nm (figure 7b). We have carried out detailed magnetic studies of manganese oxalate nanorods as well as the various manganese oxides [21]. The high-temperature susceptibility for manganese oxalate yields a Weiss temperature of $\Theta = -36$ K and an effective moment of 5.8 μ_B, consistent with Mn^{2+}. A sharp magnetic transition is observed near 15 K. This temperature is somewhat higher than the reported Néel temperature T_N of manganese oxalate (2.6 K) [31]. However, previous studies have also found a peak in the susceptibility at a temperature much above T_N [31]. This has been attributed to the presence of linear spin chains in the system. In MnO nanoparticles (28 nm) the high-temperature susceptibility yields $\Theta = -400$ K and an effective moment of 4.9 μ_B. The effective moment is somewhat less than that expected for Mn^{2+}. Bulk MnO has an antiferromagnetic transition at 118 K [32], but there is no indication of any magnetic transition in the neighborhood of T_N, just a deviation from linearity in the Curie plot.

4. Conclusions

Nanoparticles of $BaTiO_3$ in the range of 25–30 nm were obtained at 800°C by the reverse-micellar route avoiding Ba-alkoxide as the starting material. The grain size is quite stable on sintering (∼80 nm at 1100°C). The dielectric constant obtained for $BaTiO_3$ sintered at 1100°C is around 560 and the dielectric loss is 0.02 at 100 kHz. Orthorhombic Ba_2TiO_4 (normally stable at higher temperatures) with an average grain size of 40–50 nm is stabilized at room temperature using reverse micelles after heating at 1000°C. Manganese oxalate nanorods provide a convenient source to different manganese oxides, viz. MnO, Mn_2O_3 and Mn_3O_4 nanoparticles depending on the synthetic condition. CuO nanoparticles (80 nm) show enhanced magnetic susceptibility and weak ferromagnetism at 220 K.

Acknowledgement

AKG thanks the Department of Science & Technology, Govt. of India, for financial support. TA thanks CSIR, Govt. of India for a fellowship.

References

[1] G H Haertling, *J. Am. Ceram. Soc.* **82**, 797 (1999)
[2] R L Goldberg and S W Smith, *IEEE Trans. Ultrason. Ferrolectr. Freq. Control.* **41**, 761 (1994)
[3] B Jaffe Jr., W R Cook and H Jaffe, *Piezoelectric ceramics* (Academic Press, New York, 1971)
[4] K Uchino, *Acta Mater.* **46**, 3745 (1998)
[5] O Auciello, J F Scott and R Ramesh, *Phys. Today* **51**, 22 (1998)
[6] S S Chandatreya, R M Fulath and J A Pask, *J. Am. Ceram. Soc.* **64**, 422 (1981)
[7] F Selimi, S Komarneni, V K Varadan and V V Varadan, *Mater. Lett.* **10**, 235 (1990)
[8] R Asiaie, W Zhu, S A Akbar and P K Dutta, *Chem. Mater.* **6**, 123 (1996)

[9] I W Chen and X H Wang, *Nature (London)* **404**, 168 (2001)
[10] M A Sekar, G Dhanraj, H L Bhatt and K C Patil, *J. Mater. Sci.* **3**, 237 (1992)
[11] K R M Rao, A V P Rao and S Komareni, *Mater. Lett.* **28**, 463 (1996)
[12] T R N Kutty and R Balachandran, *Mater. Res. Bull.* **19**, 1479 (1984)
[13] C K Kwok and S B Desu, *J. Mater. Res.* **8**, 339 (1993)
[14] H Hirashima, E Onishi and M Nakagowa, *J. Non-Cryst. Solids* **121**, 404 (1990)
[15] M P Pechini, US Patent No. 330697 (1967)
[16] M Kakihana, M Arima, Y Nakamura, M Yashima and M Yoshimura, *Chem. Mater.* **11**, 438 (1998)
[17] P R Arya, P Jha and A K Ganguli, *J. Mater. Chem.* **13**, 415 (2003)
[18] P R Arya, P Jha, G N Subbanna and A K Ganguli, *Mater. Res. Bull.* **38**, 617 (2003)
[19] P Kumar and K L Mittal, *Handbook of microemulsions science and technology* (Marcel Dekker, New York, 1999) part III, pp. 457–742
L M Liz-Marzan and P V Kamat, *Nanoscale materials* (Kluwer Academic Publishers, London, 2003) p. 135
[20] T Ahmad, G Kavitha, C Narayana and A K Ganguli, *J. Mater. Res.* **20**, 1415 (2005)
[21] T Ahmad, K V Ramanujachary, S E Lofland and A K Ganguli, *J. Mater. Chem.* **14**, 3406 (2004)
[22] T Ahmad and A K Ganguli, *J. Mater. Res.* **19**, 2905 (2004)
[23] Y G Wang, W L Zhong and P L Zhang, *Solid State Commun.* **90**, 329 (1994)
[24] J Junquera and P Ghosez, *Nature (London)* **422**, 506 (2003)
[25] T Ahmad, R Chopra, K V Ramanujachary, S E Lofland and A K Ganguli, *Solid State Sci.* **7**, 891 (2005)
[26] C B Azzoni, A Paleari and G B Parravicini, *J. Phys. Condens. Matter* **4**, 1359 (1992)
[27] M O'Keefe and F S Stone, *J. Phys. Chem. Solids* **23**, 261 (1962)
[28] J B Forsyth, P J Brown and B M Wanklyn, *J. Phys.* **C21**, 2917 (1988)
[29] T I Arbuzova, A A Samokhvalov, I B Smolyak, N M Chebotaev and S V Naumov, *JETP Lett.* **50**, 34 (1989)
[30] K Muraleedharan, C K Subramanian, N Venkataramani, T K Gundu Rao, C M Srivastava, V Sankaranarayan and R Srinivasan, *Solid State Commun.* **76**, 727 (1990)
[31] I Sledzinska, A Murasik and P Fischer, *J. Phys.* **C20**, 2247 (1987)
[32] G H Lee, S H Huh, J W Jeong, B J Choi, S K Kim and H C Ri, *J. Am. Chem. Soc.* **124**, 12094 (2002)